Preparation and Properties of Oxadiazole-Containing Polyacetylenes as Electron Transport Materials

XIN WANG,[1,2] SHANYI GUAN,[1] HONGYAO XU,[1,3] XINYAN SU,[1] XUHUI ZHU,[4] CHUN LI[4]

[1]College of Material Science and Engineering and State Key Laboratory of Chemical Fibers and Polymeric Materials, Donghua University, Shanghai 201620, People's Republic of China

[2]School of Chemistry, Chizhou University, Chizhou 247000, People's Republic of China

[3]State Key laboratory of Crystal Material, Shandong University, Jinan 250100, People's Republic of China

[4]Institute of Polymer Optoelectronic Materials and Devices, Key Laboratory SPA-OXAcial Functional Materials, MOE, South China University of Technology, Guangzhou 510640, People's Republic of China

Received 19 November 2009; accepted 17 December 2009
DOI: 10.1002/pola.23904

ABSTRACT: A series of functional polyacetylenes (PAs) bearing diphenyl oxadiazole pendant groups (**P1**–**P4**) were prepared, and the resultant polymers are completely soluble in common organic solvents. Their structures and properties were characterized and evaluated by DSC, TGA, UV, PL, CV, and EL analyses. The results show that all the resulting polymers possesses low LUMO energy level and high thermal stability, and the resultant functional polyacetylenes without spacer group between the polyacetylene conjugated main chain and oxadiazole pendant groups (**P1**–**P3**) show lower LUMO energy level (∼−3.87 eV) and higher thermal properties (T_g) than that (**P4**) with a flexible spacer. The resultant polymer (**P2**) was applied as an ETM in bilayer electroluminescent devices and effectively enhances external quantum efficiency and the brightness of device, and decreases turn-on voltages of devices. © 2010 Wiley Periodicals, Inc. J Polym Sci Part A: Polym Chem 48: 1406–1414, 2010

KEYWORDS: electron transport material; light-emitting diodes; oxadiazole; polyacetylene; thermal properties

---

INTRODUCTION Organic and conjugated polymer light-emitting diodes (OLEDs) have been extensively studied during the past decade because of their potential applications in a new generation flat display and lighting technologies.[1–3] For ideal high-performance electroluminescent devices, the injection and transport balance of electrons and holes is needful.[4–9] However, most electroluminescent (EL) organic materials often show more efficiently hole injection due to the inherent richness of π-electrons in the EL materials, which results in an unbalance of charge injection in emitting layer and low device emissive efficiency. Therefore, many electron injection/transporting materials were prepared and investigated.[10–12]

Oxadiazoles turn out to be very well electron injection/transporting materials and have attracted significant attention owing to their prominent electron affinity, high photoluminescence quantum yield.[6,7,13] Unfortunately, the small oxadiazole molecules are easily crystallized over time due to joule heating during device operation,[6,14] which results in low efficiency and poor stability.[6,7,15] Compared to low-molecular-weight oxadiazole compounds, oxadiazole-containing polymers are expected to have higher T_g and less susceptible to crystallization under device operation. However, most of the aromatic polyoxadiazoles exhibits poor solubility in organic solvents.[7] Nevertheless, the incorporation of oxadiazole moieties as pendant groups into poly(methyl methacrylate) has exhibited higher T_gs and better processiblity relative to small oxadiazole molecules.[16,17] Attachment of the oxadiazole unit to the phenylene ring of poly(phenylenevinylene) also showed well electron injection/transport properties.[18]

Polyacetylenes (PA) is a prototypical linear conjugated polymer with alternating single and double bond, shows well electrically conductive after doping.[19,20] Proper structural design may tune the backbone-pendant interplay into harmony and synergy, generating new substituted PAs with novel functionalities. Recently, Xu and coworkers found that azobenzene-containing substituted polyacetylenes possess large third-order nonlinear optical susceptibility (up to 10^{-10} esu) and novel optical limiting properties.[21–25] Many other functional polyacetylenes with electro-optic activity, photonic responsiveness, and biologic compatibility have been investigated.[23,24,26–31] However, to the best of our knowledge, the functional polyacetylenes with electron transport properties were less investigated.

Correspondence to: H. Xu (E-mail: hongyaoxu@163.com)
Journal of Polymer Science: Part A: Polymer Chemistry, Vol. 48, 1406–1414 (2010) © 2010 Wiley Periodicals, Inc.

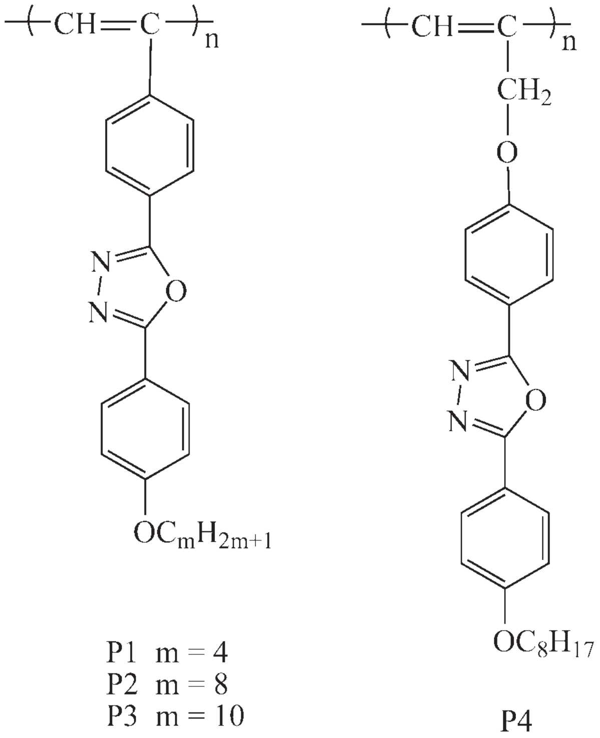

CHART 1 The structures of **P1–P4**.

In this work, a series of oxadiazole-containing PAs (Chart 1) with different terminal alkoxyl group ([HC = C—C_6H_4—C_2N_2O—C_6H_4—OC_mH_{2m+1}]$_n$, m = 4, 8, 10 for **P1, P2, P3,** respectively) or with a spacer group (OCH_2) and a terminal alkoxyl group at same time ([HC = C—OCH_2—C_6H_4—C_2N_2O—C_6H_4—OC_8H_{17}]$_n$, **P4**) were prepared. Their structure and properties are to be characterized and evaluated. The application of **P2** as electron injection materials in bilayer electroluminescent devices will be examined.

EXPERIMENTAL

Materials

Monomer molecules (**M1–M4**) were synthesized according to the Scheme 1 and refs. 27,30–32. The red emissive material, 4,7-di (5-3,5-bis(naphthalene-1-yl)phenyl-4-hexylthiophen-2-yl)-2,1,3-benzothiadiazole (DB) was prepared based on ref. 33. Poly(ethylenedioxythiophene): poly(styrene sulfonate) (PEDOT:PSS) was used as hole transport layers and also serve to planarise the anode.[7] Acetonitrile, tetrabutylammonium perchlorate (n-Bu)$_4NClO_4$ (TBAP) (99%) (Fluka), PEDOT (Bayer), and all the other reagents and solvents were used as received.

Instruments

Thermal analyses were performed on a TA Iinstruments DSC 9000 for differential scanning calorimetry (DSC) under nitrogen at a scan rate was 10 °C/min within the temperature range 30–300 °C.

Cyclic voltammetry (CV) was determined on a LK98C electrochemical analyzer at a scanning rate of 50 mV/s, which was equipped with a three-electrode cell. Pt wire was used as a counter electrode and an Ag/Ag^+ was used as a reference electrode in the CV measurement. The polymer thin films were cast onto a carbon-glass of a working electrode. The measurements were carried out at room temperature and the electrolyte of 0.1 M TBAP in acetonitrile with nitrogen-saturated.

Absorption spectra were recorded on a Shimadzu UV-265 spectrometer and fluorescence spectra were obtained on a Shimadzu RF-5301PC spectrofluorimeter.

The luminance properties of the devices were measured with a photodiode calibrated by a Spectra Scan Spectrophotometer. External quantum efficiency (EQE) was verified by measuring in the integrating sphere after encapsulation of the devices with UV-cured epoxy and thin cover glass. Current-brightness-voltage characteristics were made by using a keithley source measurement unit (Keithley 2400 and 2000) with a calibrated silicon photodiode. The EL spectra were measured by JY SPEX CCD 3000 spectrometer. All the measurements were carried out in ambient atmosphere at room temperature.

Polymerization

All the polymerization reactions and manipulations were performed under prepurified nitrogen using Schlenk techniques either in vacuum-line system of an inert-atmosphere glove box, except for the purification of the polymers, which were done in open air. Typical procedure for the polymerization is given below: Into a baked 20-mL Schlenk tube with a side arm was added 1 mmol of the monomer. The tube was evacuated under vacuum and then flushed with dry nitrogen three times through the side arm. Dioxane (3 mL) was injected into the tube to dissolve the monomer. The catalyst solution was prepared in another tube by dissolving 4.6 mg (0.01 mmol) $[Rh(nbd)Cl]_2$ and 2.02 mg (0.02 mmol) Et_3N in 2 mL of dioxane, which was transferred to the monomer solution using a hypodermic syringe. The reaction mixture was stirred at 60 °C under nitrogen for 6 h. The mixture was then diluted with 5 mL of dioxane and added dropwise to 200 mL of methanol under stirring. The precipitate was centrifuged and redissolved in THF. The THF solution was added dropwise into 200 mL of methanol to precipitate the polymer. The dissolution–precipitation process was repeated three times, and the finally isolated precipitant was dried under vacuum at 30 °C to a constant weight.

2-(4-Butyloxyphenyl)-5-(4-ethynylphenyl)-1,3,4-oxadiazole (M1)

FTIR (KBr, ν cm^{-1}): 3280, 2952, 2879, 2100, 1612, 1495, 842. ^{1}H-NMR (300 MHz, $CDCl_3$, δ, ppm): 0.87 (t, 3H, CH_3), 1.48 (m, 2H, CH_2CH_3), 1.84 (m, 2H, OCH_2CH_2), 3.24 (s, 1H, $\equiv CH$), 4.05 (t, 2H, OCH_2), 7.02 (d, 2H, J = 8.8 Hz, Ar-H), 7.64 (d, 2H, J = 8.3 Hz, Ar-H), 8.05 (d, 2H, J = 8.9 Hz, Ar-H), 8.09 (d, 2H, J = 8.4 Hz, Ar-H). ^{13}C-NMR (100.61 MHz, $CDCl_3$, δ, ppm): 164.5, 163.4 (Oxa-C), 157.4, 132.8, 127.1, 126.6, 125.8, 122.5, 117.6, 114.9 (Ar-C), 82.3 ($C\equiv CH$), 79.9 ($\equiv CH$), 68.5 (OCH_2), 31.8 (OCH_2CH_2), 19.1 (CH_2CH_3), 14.1 (CH_3).

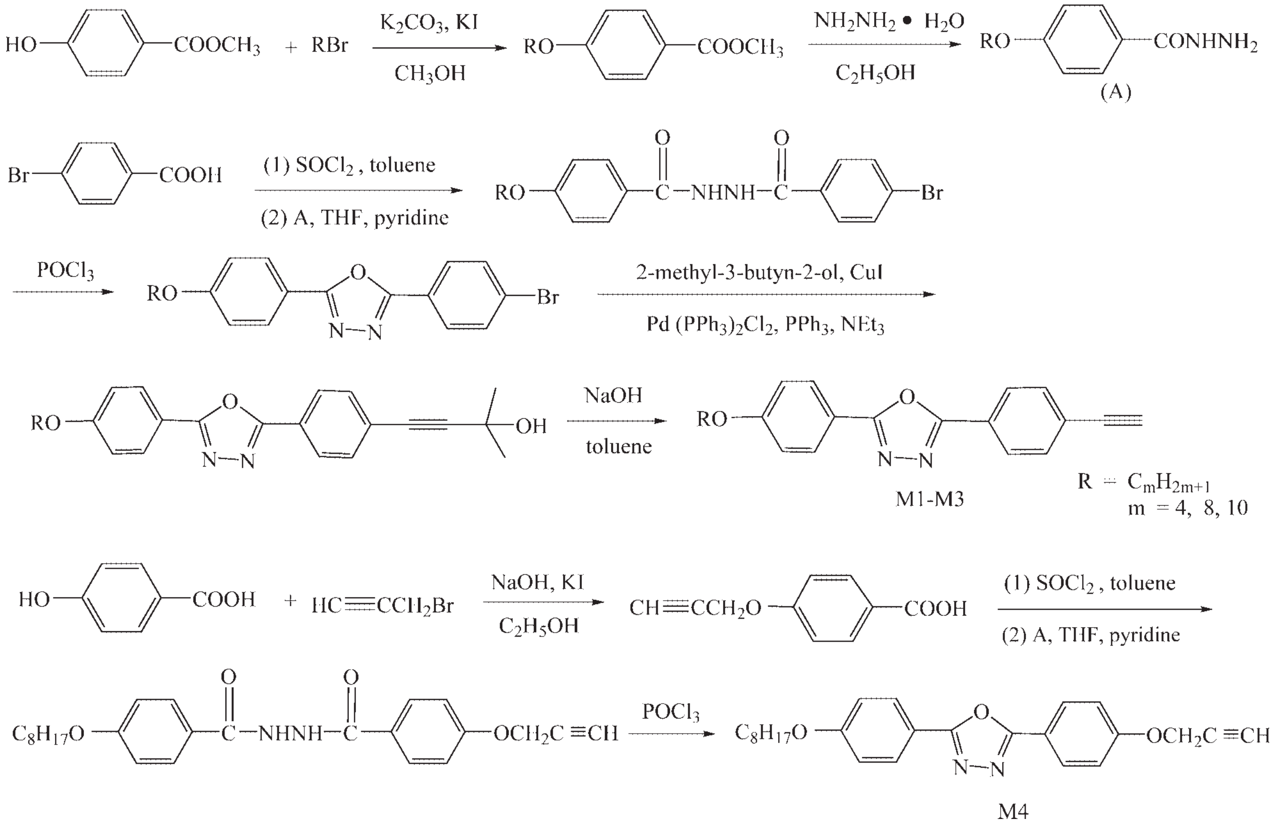

SCHEME 1 The synthesis routes of monomer molecules (**M1–M4**).

2-(4-Octoxyphenyl)-5-(4-ethynylphenyl)-1,3,4-oxadiazole (M2)

FTIR (KBr, ν cm^{-1}): 3272, 2932, 2851, 1611, 1456, 843. ^{1}H-NMR (300 MHz, $CDCl_3$, δ, ppm): 0.88 (t, 3H, CH_3), 1.35 (m, 10H, $(CH_2)_5CH_3$), 1.83 (m, 2H, OCH_2CH_2), 3.24 (s, 1H, $\equiv CH$), 4.04 (t, 2H, OCH_2CH_2), 7.03 (d, 2H, J = 8.9 Hz, Ar-*H*), 7.68 (d, 2H, J = 8.4 Hz, Ar-*H*), 8.07 (m, 4H, Ar-*H*). ^{13}C-NMR (100.61 MHz, $CDCl_3$, δ, ppm): 164.8, 163.5 (Oxa-*C*), 162.1, 132.7, 128.7, 126.6, 125.3, 124.1, 116.0, 115.0(Ar-*C*), 82.8 ($C\equiv CH$), 79.9 ($\equiv CH$), 68.3(OCH_2), 31.8(OCH_2CH_2), 29.1–29.3 ($OC_2H_5C_3H_6C_3H_7$), 26.0 ($CH_2C_2H_5$), 22.7(CH_2CH_3), 14.1 (CH_3).

2-(4-Decyloxyphenyl)-5-(4-ethynylphenyl)-1,3,4-oxadiazole (M3)

FTIR (KBr, cm^{-1}): 3273, 2920, 2851, 2100, 1611, 1456, 843. ^{1}H-NMR (300 MHz, $CDCl_3$, δ, ppm): 0.87 (t, 3H, CH_3), 1.25–1.48 (m, 14H, $(CH_2)_7CH_3$), 1.83 (m, 2H, OCH_2CH_2), 3.25 (s, 1H, $\equiv C{-}H$), 4.04 (t, 2H, OCH_2), 7.02 (d, 2H, J = 8.9 Hz, Ar-*H*), 7.64 (d, 2H, J = 8.5 Hz, Ar-*H*), 8.08 (m, 4H, Ar-*H*). ^{13}C-NMR (100.61 MHz, $CDCl_3$, δ, ppm): 164.5(Oxa-*C*), 157.4, 132.7, 128.3, 127.1, 125.6, 122.1, 117.5, 114.9(Ar-*C*), 82.3 ($C\equiv CH$), 79.9 ($\equiv CH$), 68.6(OCH_2), 31.8($CH_2C_2H_5$), 29.3–26.0 ($OCH_2C_6H_{12}$), 22.7(CH_2CH_3), 14.1 (CH_3).

2-(4′-Octoxyphenyl)-5-(4′-propynyloxyphenyl) -1,3,4-oxadiazole (M4)

FTIR (KBr, cm^{-1}): 3270, 2922, 2853, 2127, 1612, 1497, 837. ^{1}H-NMR (300 MHz, $CDCl_3$, δ, ppm): 0.88 (t, 3H, CH_3); 1.23 (m, 10H, $(CH_2)_5CH_3$), 1.71 (m, 2H, OCH_2CH_2), 2.54 (s, 1H, $\equiv CH$), 3.94 (t, 2H, OCH_2CH_2), 4.78 (s, 2H, $CH_2C\equiv$), 7.1 (m, 4H, J = 7.62 Hz and J = 8.86 Hz, Ar-*H*), 8.05 (m,4H, J = 7.62 Hz and J = 8.86 Hz, Ar-*H*). ^{13}C-NMR (100.61 MHz, $CDCl_3$, δ, ppm): 164.3, 163.9 (Oxa-*C*), 161.9, 160.0, 128.6, 117.6, 116.3, 115.4, 115.0 (Ar-*C*), 78.0 ($C\equiv CH$), 75.2($\equiv CH$), 68.3 (OCH_2), 55.9 ($OCH_2C\equiv$), 31.8 ($CH_2C_2H_5$), 29.3–26.0 ($OCH_2C_4H_8$), 22.7 (CH_2CH_3),14.1 (CH_3).

Poly(2-(4-butyloxyphenyl)-5-(4-ethynylphenyl)-1,3,4-oxadiazole) (P1)

Yellow solid, yield 92%, $M_w = 2.93 \times 10^4$, $M_w/M_n = 1.36$ (polystyrene calibration). FTIR (KBr, ν cm^{-1}): 3045, 2925, 2857, 1613, 1496, 837. ^{1}HNMR (300 MHz, $CDCl_3$, δ, ppm): 0.96 (br, CH_3), 1.45 (br, CH_2CH_3), 1.90 (br, OCH_2CH_2), 3.82 (br, OCH_2), 5.92(br, *cis* = C-*H*), 6.67 (br, Ar-*H* and *trans* = C-*H*), 6.91 (br, Ar-*H*), 7.67 (br, Ar-*H*). ^{13}C-NMR (100.61 MHz, $CDCl_3$, δ, ppm): 164.3–163.7 (Oxa-*C*), 134.9 ($C{=}CH$), 128.8–127.7(Ar-*C*), 123.9 ($C{=}CH$), 115.0–114.9 (Ar-*C*), 68.5 (OCH_2), 31.8 (OCH_2CH_2), 19.1 (CH_2CH_3), 14.1 (CH_3).

Poly(2-(4-octoxyphenyl)-5-(4-ethynylphenyl)-1,3,4-oxadiazole) (P2)

Yellow black solid, yield 95%, $M_w = 3.19 \times 10^4$, M_w/M_n = 1.42 (polystyrene calibration). FTIR (KBr, ν cm^{-1}): 2925, 2854 (CH_2, CH_3), 1612, 1496 (C=C), 837 (*p*-Ar). ^{1}H-NMR (300 MHz, $CDCl_3$, δ, ppm): 0.88 (br, CH_3), 1.28 (br, $(CH_2)_5CH_3$), 1.75 (br, OCH_2CH_2), 3.90 (br, OCH_2), 5.98 (br, *cis* = C-*H*), 6.72 (br, Ar-*H* and *trans* = C-*H*), 6.89 (br, Ar-*H*), 7.67 (br, Ar-*H*). ^{13}C-NMR (100.61 MHz, $CDCl_3$, δ, ppm): 164.3–163.7 (Oxa-*C*), 134.9

(C=CH), 128.8–127.7(Ar-C), 123.9 (C=CH),115.0–114.9 (Ar-C), 68.3 (OCH$_2$), 31.8 (CH$_2$C$_2$H$_5$), 29.6–26.0 (OCH$_2$$C_4H_8$), 22.7 ($CH_2CH_3$), 14.1 ($CH_3$).

Poly(2-(4-decyloxyphenyl)-5-(4-ethynylphenyl)-1,3,4-oxadiazole) (P3)

Yellow black solid, yield 98%, $M_w = 2.54 \times 10^4$, $M_w/M_n = 1.71$ (polystyrene calibration). FTIR (KBr, v cm^{-1}): 2926, 2855(CH$_2$, CH$_3$), 1611, 1496(C=C), 838(p-Ar). ^{1}H-NMR (300 MHz, CDCl$_3$, δ, ppm): 0.87 (br, CH_3), 1.26 (br, (CH_2)$_7$CH$_3$), 1.70 (br, OCH$_2$CH_2), 3.83 (br, OCH_2), 5.92 (br, *cis* = C-H), 6.68 (br, Ar-H and *trans* = C-H), 6.93 (br, Ar-H), 7.69 (br, Ar-H). ^{13}C-NMR (100.61 MHz, CDCl$_3$, δ, ppm): 164.3–163.7 (Oxa-C), 134.9 (C=CH), 128.8–127.7(Ar-C), 123.9 (C=CH), 115.0–114.9 (Ar-C), 68.8 (OCH$_2$), 31.8 (CH$_2$C$_2$H$_5$), 29.7–25.9 (OCH$_2$$C_6H_{12}$), 22.7 ($CH_2CH_3$), 14.1 ($CH_3$).

Poly(2-(4′-octoxyphenyl)-5-(4′-propynyloxyphenyl)-1,3,4-oxadiazole) (P4)

Brown black solid. Yield: 25%. $M_w = 2.67 \times 10^4$, $M_w/M_n = 1.53$ (polystyrene calibration). FTIR (KBr, v cm^{-1}): 2923, 2854 (CH$_2$, CH$_3$), 1611, 1497 (C=C), 839 (p-Ar). ^{1}H-NMR (300 MHz, CDCl$_3$, δ, ppm): 0.89 (br, CH_3), 1.31 (br, (CH_2)$_5$CH$_3$), 1.76 (br, OCH$_2$CH_2), 3.96 (br, OCH_2), 5.2 (br, OCH_2CH=), 6.85 (br, Ar-H and trans = C-H), 7.36 (br, Ar-H). ^{13}C-NMR (100.61 MHz, CDCl$_3$, δ, ppm): 164.3, 163.2 (Oxa-C), 161.6, 144.3(Ar-C), 139.2 (C—CH), 128.4, 126.4 (Ar-C), 123.0 (C—CH), 115.7 (Ar-C), 68.1(C,OCH$_2$C$_7$H$_{15}$), 66.3 (CH$_2$ C=), 31.8 (CH$_2$C$_2$H$_5$), 29.7–26.0 (OCH$_2$$C_4H_8$), 22.6 ($CH_2CH_3$), 14.1 ($CH_3$).

Device Fabrication

The bilayer blended devices [ITO/PEDOT:PSS (50 nm)/PVK(40 nm)/DB:**P2** (80 nm)/Ba(4 nm)/Al(200 nm)] using a poly(vinylcarbazole) (PVK) as a hole transport material layer, and a mixture of DB and **P2** as the emitting and electron transfer film layer were prepared. The fabrication process of the diodes followed a standard procedure below. The patterned indium-tin oxide (ITO, 15 Ω/square) coated glass substrates were cleaned with acetone, detergent, distilled water and 2-propanol, successively in an ultrasonic bath. After treatment with oxygen plasma, PEDOT: PSS was spin-coated onto the ITO substrate and dried in a vacuum oven at 80 °C for 8 h. PVK was coated on top of a dried PEDOT:PSS layer. Subsequently, a thin film of the emitting layer was coated from a mixed toluene solution (35 mg/mL) at different ratio of DB:**P2,** 100:0, 90:10, and 80:20 (wt/wt), inside a glove box under vacuum, respectively. As PVK is barely soluble in toluene, it remains unperturbed upon deposition of the top emitting layer. Then, a thin layer of barium as an electron injection cathode, and aluminum protection layer were thermally deposited by vacuum evaporation through a mask under 10^{-4} Pa. The deposition speed and thickness of the barium and aluminum layers were monitored with a thickness/rate meter. The cathode area is defined as the active area of the device, typically, 0.17 cm^2 in this study. All steps except PEDOT:PSS layer were performed in N$_2$-filled dry boxes.

RESULTS AND DISCUSSION

Syntheses and Solubility of the Polymers

All polymerization reactions were carried out under nitrogen atmosphere using a standard Schlenk vacuum-line system. We first synthesized functional polyacetylene (PA) containing oxadiazole group without spacer and alkoxyl tail and found that the resultant PA is insoluble in common organic solvent. However, the functional PAs bearing oxadiazole with alkoxyl tail (—OC$_m$H$_{2m+1}$, $m = 4, 8, 10$ for **P1, P2, P3,** respectively) are soluble in common organic solvent, hinting that introduction of flexible terminal group obviously improve the solubility of resulting polymers. Similar phenomena were also observed in our previous work on azobenzene-containing PAs.[24] Furthermore, it is found that the solubility of resultant PAs is affected by the length of the flexible terminal chain, and increases with the flexible terminal alkoxyl chain length. For example, polyacetylene **P1** with short terminal alkoxyl chain ($m = 4$) is partial soluble in common organic solvent such as THF, CHCl$_3$, toluene and dioxane, and **P2**–**P4** with long flexible terminal alkoxyl group ($m = 8$ or 10) completely soluble in above common organic solvents and also display well film-forming properties. Therefore, the structures of resultant polymers can be characterized by solution spectral methods.[30,31]

Structure Characterization

The structures of **P1**–**P4** were characterized by spectroscopic techniques, such as FTIR and ^{1}H-NMR, and they all gave satisfactory spectra data corresponding to their expected molecular structures. For example, the characteristic ≡C—H and C≡C absorption bands of the monomers completely disappear in the IR spectra of their polymers, proving that the C≡C bond of monomers have transformed to C=C unit of resulting polymers. All the characteristic proton resonance absorption bands in the ^{1}H-NMR spectra of resulting polymers (**P1**–**P4)** significantly change broad and the new broad resonance absorption band located at about δ 5.9 or 6.8 corresponding to the *cis* or *trans* olefin absorption of the PAs appears in the spectra of resultant polymers compared with the spectra of the monomers, which also further confirms that the C≡C unit has transferred to C=C bond. According to Percec and coworkers method,[34–40] we quantified the *cis* content of the polymers based on the following equation:

$$cis\text{ content }(\%) = [A_{5.92}/((A + A_{5.92})/9)] \times 100 \qquad (1)$$

where $A = A_{7.69} + A_{6.93} + A_{6.68}$, corresponding to the peak areas of the eight aryl protons of the polymers and the peak areas of *trans* olefinic proton, and $A_{5.92}$ corresponds to the peak areas of *cis* olefinic proton. Then, the *cis* olefin contents can be estimated based on integration areas of the peak, i.e., the *cis* contents of **P1**, **P2**, and **P3** are 93.1, 96.4, and 81.8%, respectively. Similar to **P1**–**P3**, the *cis* content of **P4** is 43.3%. The low *cis* content of **P4** may result from the *cis*-*trans* isomerization during the polymerization due to the small stereo-hinder of the flexible ether group as spacer.[41] The characteristic acetylene and propargyl carbons of the monomer resonances were not found, and two new peaks

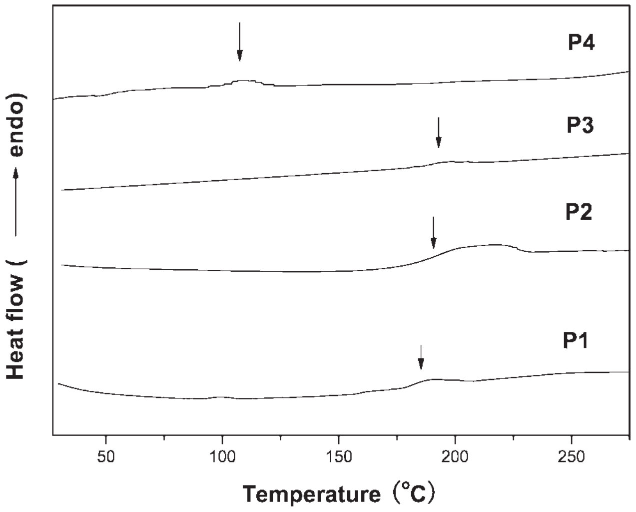

FIGURE 1 DSC curve (measured under N_2 at a heating rate of 20 °C/min) of **P1–P4**.

associated with the resonances of the olefin carbon atoms of the PA backbone were, however, observed in the ^{13}C-NMR spectra of these polymers, further substantiating the molecular structure of these polymers. In addition, the GPC measurement results confirm that all the polymers show high average molecular weights, further indicating that the polymers are obtained[30,31] and the detailed data have been given in experimental section.

Thermal Stability

Thermal stability of polymer is very important for device longevity. The glass transition temperatures (T_gs) of resultant polymers were determined by a differential scanning calorimeter (DSC) in nitrogen atmosphere at a heating rate of 20 °C/min. Figure 1 displays the DSC curve of the polymers and their T_gs are summarized in Table 1. As shown in Figure 1, the T_gs of **P1**, **P2**, **P3**, and **P4** are shown at 194.6, 193.3, 187.1, and 104.8 °C, respectively. **P1–P3** exhibited the higher T_g than **P4**, which may be attributed to stronger electron interaction between main chain and substituted inside group.[42,43] From Table 1, it is also found that the T_gs of the resultant polymers **(P1–P3)** increase with decrease of alkoxyl chain length.

The TGAs of **P1–P4** are measured and the data are also listed in Table 1. From Table 1, these polymers display very high thermal stability in nitrogen and their T_ds are up to more than 330 °C (T_d, 5% loss weight). To prove the thermal stability, we made TGA-FTIR experimental and investigated the UV spectra of the pristine **P1-P4** film annealed under ambient atmosphere at 200 °C for 30 min. The results show no obvious IR absorption from decomposed product and the UV absorption pattern and profile of polymer films don't appear any obvious changes before 200 °C, implying that no significant molecular decomposition and isomerization happens at the condition. The high thermal stability may be due to the reason that the backbones of **P1–P4** are surrounded by a rigid diaryl oxadiazole groups with high thermal properties to shield the polymer main chains from the thermal attack.[27,28,30,32,44] Similar phenomena was found by Percec and coworkers.[41,45] When the polymers were heated to more than 200 °C, some weak aromatic FTIR spectral absorption were observed, which may be originated from the decomposition induced by backbone isomerization of polyacetylene.[38,41,45] The detailed thermal decomposition mechanism is in progress, which will be reported in our future publication. Simultaneously, it is found that the PAs directly bearing oxadiazole groups (**P1–P3**) also exhibit higher T_d than that with a spacer between PA main chain and oxadiazole pendant (**P4**). This is consistent with the results of the DSC measurement.

Optical Properties

The UV-vis absorption spectra of all polymers in film are shown in Figure 2 and the data are summarized in Table 1. Taken the absorption spectrum of **P2** as an example, **P2** in neat film shows maximal absorption peak at 322 nm, corresponding to the side chain aromatic oxadiazole group.[43] The absorption edge is measured to be 391 nm, from which the π–π* band gap energy is estimated to be 3.17 eV. It is seen from Table 1 that the band gap energies decrease with increasing alkoxyl chain length. Moreover, it is found that the PAs directly bearing oxadiazole groups (**P1–P3**) display lower band gap energy than that with a spacer group (**P4**) owing to larger π-electron conjugation effect in the former than the latter.[46,47]

Figure 2 also shows the PL spectra of **P1–P4** in the film on quartz. The photoluminescence spectra were obtained after excitation at the absorption maxima of the oxadiazole moiety

TABLE 1 The Properties of **P1–P4**

Sample	λ_{abs} (nm)[a]	E_g^{opt} (eV)[b]	λ_{max}^{PL} (nm)[a]	E_{onset} (V)[c]	E_{LUMO} (eV)[d]	E_{HOMO} (eV)[d]	T_d (°C)[e]	T_g (°C)[f]
P1	325	3.25	426	−0.37	−4.03	−7.28	346	194.6
P2	322	3.17	424	−0.43	−3.97	−7.14	379	193.3
P3	318	3.16	418	−0.53	−3.87	−7.03	353	187.1
P4	301	3.51	433	−1.12	−3.28	−6.79	337	104.8

[a] The maximum absorption or emission wavelength.

[b] Estimated from the absorption edge of the polymers.

[c] E_{onset} is onset potential of polymer, measured in 0.1 M TBPA/CH_3CN, scan rate 50 mV/s.

[d] Estimated from $E_{LUMO} = -(E_{red}^{onset} + 4.4)$ eV and $E_{HOMO} = (E_{LUMO} - E_g^{opt})$ eV).

[e] T_d measured under nitrogen at a heating rate of 10 °C/min (5% loss weight).

[f] T_g measured under nitrogen at a heating rate of 20 °C/min.

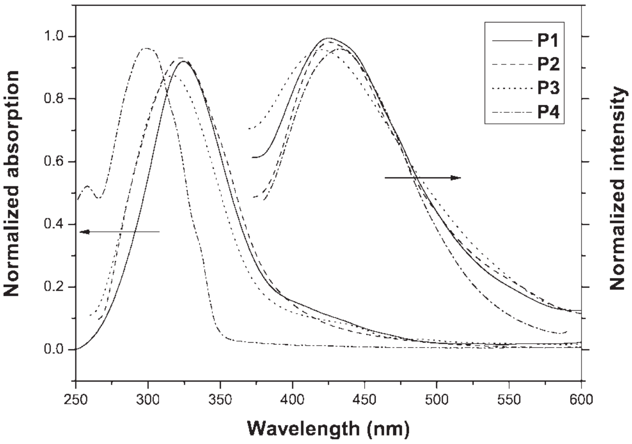

FIGURE 2 The UV-vis absorption and PL spectra of **P1–P4** in the film on quartz.

(322 nm). The maximal emission wavelengths of **P1–P4** are listed in Table 1. It can be seen from Table 1 that, similar with UV spectra, maximal photoluminescence peak wavelength also decreases with increasing alkoxyl chain length.

Electrochemical Properties

To order to match the energy band structural Scheme 2 of PLED device, it is necessary to determine the energy levels of the lowest unoccupied molecular orbital (LUMO) and the highest occupied molecular orbital (HOMO) of each component. Cyclic voltammetry was employed to investigate the redox behavior of the polymer **P1–P4** and estimate the HOMO and LUMO energy levels of the polymers. As a comparison, the redox behavior of **M2** (the corresponding monomer of **P2**) was investigated under the same conditions. The cyclic voltammograms of **P2**, **P4**, and **M2** are depicted in Figure 3 and energy level data of all polymers are summarized in Table 1. During the cathodical scan, **M2** exhibits two reduction peaks at −1.33 and −2.28 V, respectively, and the onset potential is at −1.10 V. However, **P2** shows two irreversible reduction peaks at −0.83 and −1.62 V, respectively, and onset potential is at −0.43 V. The onset potentials of the *n*-doping processes in a conjugated polymer can be utilized as a surrogate to estimate the LUMO energy levels[5] according to the empirical equation,[6] $E_{\mathrm{LUMO}} = -(E_{\mathrm{red}}^{\mathrm{onset}} + 4.4)$ eV, where $E_{\mathrm{red}}^{\mathrm{onset}}$ is the onset potentials for the reduction processes of a polymer. The LUMO energy level of **P2** is thus estimated to be −3.97 eV, which is lower by −0.75 eV than that of the monomer **M2** (−3.23 eV), hinting that **P2** has well electron injection property. The value is almost similar to that of PPV-OXD (−3.93 eV) and its derivate (−3.98 eV).[18] During the cathodical scan, however, the CV curve of **P4** shows onset potential is at −1.12 V, the corresponding LUMO energy level is at −3.28 eV. In addition, the LUMO energy level of **P2** (−3.93 eV) is significantly lower than that of **P4** (−3.28 eV), hinting that the former has larger π-electron conjugation than the latter. It is also consistent with the result of UV spectra.[8,48] Similar results are observed in **P1** and **P3,** that is, the directly incorporation of PA into oxadizaole (Chart 2) not only provides a continuous conduction path through the *p*-orbital overlapping along the polymer backbone but also facilitate the generation of charge carriers by either partial oxidation (i.e., *p*-doping) or partial reduction (i.e., *n*-doping).[8,43,48,49] Moreover, the HOMO energy levels are also evaluated based on optical band gap from UV-vis spectra and the LUMO energy level and the results are summarized in Table 1. From Table 1, the HOMO energy levels of all polymers are very low. It is favor to blocking the hole transport.[43]

$$\mathrm{M1\ -\ M4} \xrightarrow[\text{1,4-Dioxane}]{[\mathrm{Rh(nbd)Cl}]_2,\ \mathrm{NEt_3}} \mathrm{P1\!-\ P4}$$

SCHEME 2 The synthesis routes of **P1–P4**.

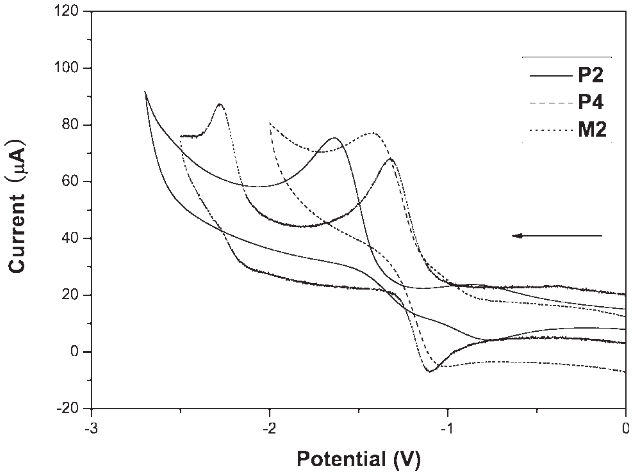

FIGURE 3 Cyclic voltammograms of **M2**, **P2**, and **P4** recorded in film (0.1 M TBPA/CH_3CN, scan rate 50 mV/s).

Application of P2 as ETM in a Bilayer Red-Light-Emitting Device

Owing to the well solubility, higher thermal stability and excellent electron injection ability or low LUMO energy level, the bilayer OLED devices with a configuration of ITO/PEDOT: PSS/PVK/DB:**P2** (x:y wt/wt)/Ba/Al] using **P2** with directly linkage between the mainchain and the pendents as ETM were prepared. To decrease the operating voltage and smooth the surface roughness of the indium tin oxide (ITO)

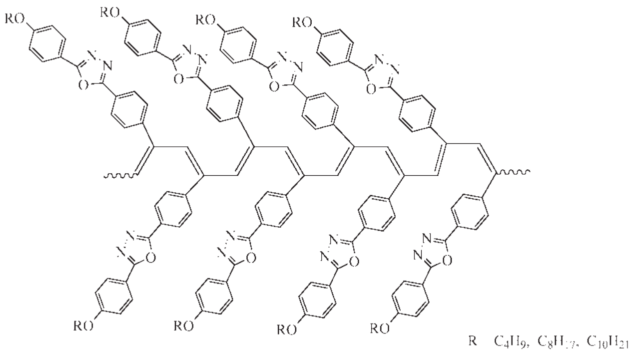

CHART 2

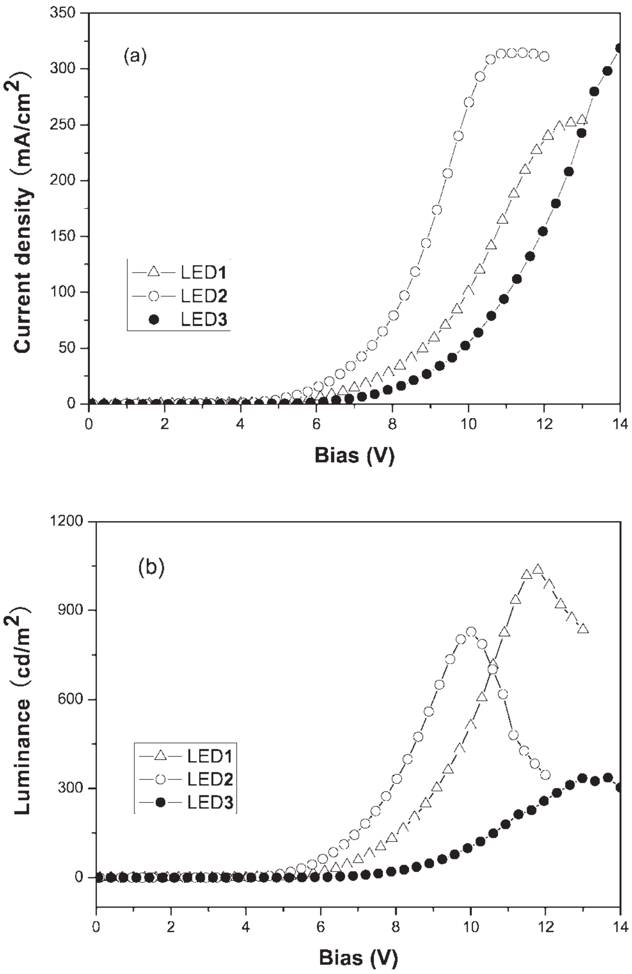

FIGURE 4 Voltage-current (**a**) and voltage-luminance (**b**) curves of ITO/PEDOT:PSS/X/Ba/Al diodes (LED**1**: X = PVK/DB, LED**2**: X = PVK/DB:**P2**(90:10), LED**3**: X = PVK/DB:**P2**(80:20)).

electrode, the hole injection-transport layer, poly(3,4-ethylenedioxythiophene) doped with poly(styrenesulfonate) (PEDOT/PSS), was spin-coated onto the surface-treated ITO substrate and dried on a hot plate for 30 min at 110 °C. The emissive material DB is an organic red emitters[33] and PVK is a hole transporting/electron blocking layer. For comparison, we firstly fabricated a bilayer LED**1** without **P2**, ITO/PEDOT:PSS/PVK/DB/Ba/Al, the operating voltage of EL emission was observed over 5.7 V with the EQE of 0.77% and the brightness of 334 cd/m^2 due to unbalanced charge injection and transport.[50,51] For improving the emissive properties of device, we used **P2** as an mixed electron-transporting materials to fabricate two bilayer devices, ITO/PEDOT: PSS/PVK/DB:**P2** (90:10 wt/wt)/Ba/Al] (LED**2**) and [ITO/PEDOT:PSS/PVK/DB:**P2** (80:20 wt/wt)/Ba/Al] (LED**3**). The film thickness of DB and **P2** were controlled to be 80 nm. In the **P2**/ DB mixture, no phase separation was observed up to the **P2** fraction of 20 wt %.

TABLE 2 LEDs Properties of **P2** Electron Transport Layer

Devices	λ_{max}^{EL}(nm)	V_{on}(V)	L_{max} (cd/m^2)	EQE (%)
LED**1**	643	5.7	334	0.77
LED**2**	649	4.1	827	1.42
LED**3**	649	4.5	1,036	1.65

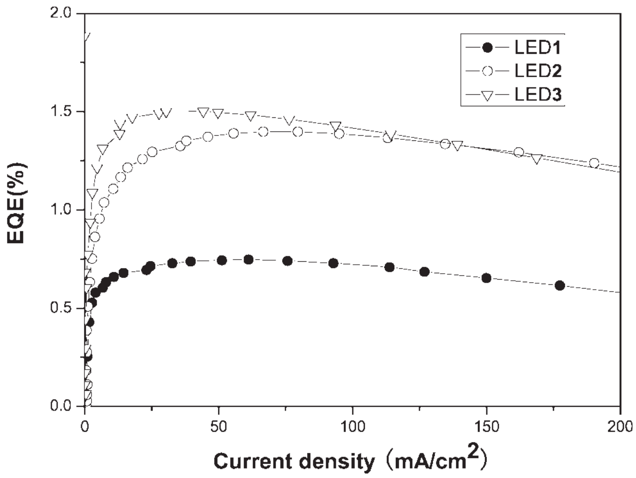

FIGURE 5 EQE as a function of current characteristics of ITO/PEDOT:PSS/X/Ba/Al diodes (LED**1**: X = PVK/DB, LED**2**: X = PVK/DB:**P2**(90:10), LED**3**: X = PVK/DB:**P2**(80:20)).

The current density-voltage (a) and luminescence-voltage (b) characteristics of LED**1**-LED**3** are shown in Figure 4 and the performances of devices are tabulated in Table 2. As can be seen in Figure 4, the turn-on voltages of LED**2** and LED**3** are about 4.1 and 4.5 V, respectively, which are significantly lower than that of LED**1** without **P2** as electron-transporting materials. The luminescence intensities of LED**2** and LED**3** also increase significantly with an increase in voltage [Fig. 4(b)]. Compared with LED**1**, the brightness increase drastically from 334 cd/cm^2 to 827 cd/cm^2 (LED**2**) and 1,036 cd/m^2 (LED**3**), respectively. Simultaneously, the higher EQE (Fig. 5) and lower turn-on voltages in LED**2** and LED **3** were

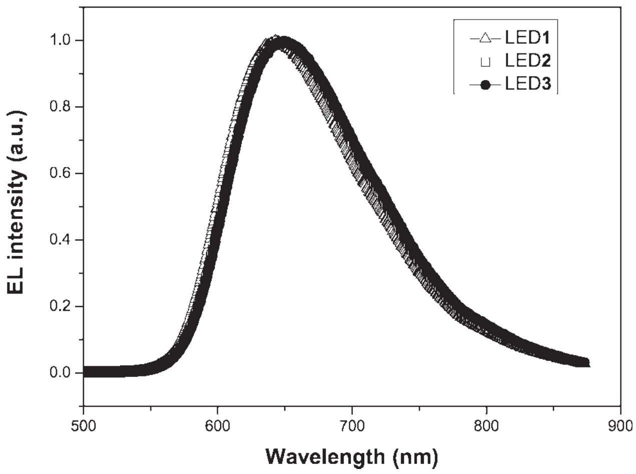

FIGURE 6 Normalized EL spectra of ITO/PEDOT:PSS/X/Ba/Al diodes (LED**1**: X = PVK/DB, LED**2**: X = PVK/DB:P2(90:10), LED**3**: X = PVK/DB:P2(80:20)).

observed, hinting that doping **P2** effectively improve the performance of devices.

Figure 6 shows the EL spectra of all LEDs at wavelength from 643 to 649 nm and all devices show deep red emission, which correspond to the intrinsic electroluminescence of DB, indicating that these ELs are mainly originated from the DB emission. That is, **P2** mainly plays as a role to improve electron injection and transport in the device.

CONCLUSIONS

A series of oxadiazole-containing polyacetylene were designed and characterized, and their properties were investigated. The incorporation of oxadiazole into PA with conjugated main chain has endowed resulting polymer with novel electron affinity (or low LUMO energy level) and high thermal properties ($T_d > 330$ °C, 5% loss weight). Their thermal properties and electron affinity increases with the flexible terminal alkoxyl chain length. The functional PAs directly bearing oxadiazole (**P2**, −3.97 eV) possess better thermal stability and lower LUMO energy level than that with a spacer group (**P4**, −3.28 eV). **P2** as ETM effectively improves the performance of bilayer LEDs, ITO/PEDOT:PSS/PVK/DB:**P2**/Ba/Al, which the external quantum efficiency (EQE) and the maximum brightness of devices are enhanced, and turn-on voltages decreases. The work may pave the way for designing new ETM with high thermal stability and well electron affinity.

Financial support from the National Natural Science Fund of China (Grant Nos. 90606011, 20974018 and 50472038), Ph.D. Program Foundation of Ministry of Education of China (No. 20070255012), Shanghai Leading Academic Discipline Project (No. B603) and Open Project of The State Key Laboratory of Crystal Materials (KF0809), the Program of Introducing Talents of Discipline to Universities (No. 111-2-04), Anhui Provincial Natural Science Foundation (No. 090414190), and Anhui Provincial University Natural Science Foundation (No. KJ2009A122).

REFERENCES AND NOTES

1 Sheats, J. R.; Antoniadis, H.; Hueschen, M.; Leonard, W.; Miller, J.; Moon, R.; Roitman, D.; Stocking, A. Science 1996, 273, 884–888.

2 Fernández, J. E. Science 2007, 315, 1807–1810.

3 Friend, R. H.; Gymer, R. W.; Holmes, A. B.; Burroughes, J. H.; Marks, R. N.; Taliani, C.; Bradley, D. D. C.; Santos, D. A. D.; Brédas, J. L.; Lögulund, M.; Salaneck, W. R. Nature 1999, 397, 121–128.

4 Cao, Y.; Parker, I. D.; Yu, G.; Zhang, C.; Heeger, A. Nature 1999, 397, 414–417.

5 Sung, H. H.; Lin, H. C. Macromolecules 2004, 37, 7945–7954.

6 Kulkarni, A. P.; Tonzola, C. J.; Babel, A.; Jenekhe, S. A. Chem Mater 2004, 16, 4556–4573.

7 Hughes, G.; Bryce, M. R. J Mater Chem 2005, 15, 94–107.

8 Chen, S. H.; Chen, Y. Macromolecules 2005, 38, 53–60.

9 Jenekhe, S. A.; Osaheni, J. A. Science 1994, 265, 765–768.

10 Lee, T.; Landis, C. A.; Dhar, B. M.; Jung, B. J.; Sun, J.; Sarjeant, A.; Lee, H.-J.; Katz, H. E. J Am Chem Soc 2009, 131, 1692–1705.

11 Zhang, X.-B.; Tang, B.-C.; Zhang, P.; Li, M.; Tian, W.-J. J Mol Struct 2007, 846, 55–64.

12 Gong, X.; Yang, Y.; Xiao, S. J Phys Chem C 2009, 113, 7398–7404.

13 Lee, R.-H.; Hsu, H.-F.; Chan, L.-H.; Chen, C.-T. Polymer 2006, 47, 7001–7012.

14 Cha, S. W.; Choi, S.-H.; Kim, K.; Jin, J.-I. J Mater Chem 2003, 13, 1900–1904.

15 Sun, Y.-M. Polymer 2001, 43, 9495–9504.

16 Strukelj, M.; Papadimitrakopoulos, F.; Miller, T. M.; Rothberg, L. J. Science 1995, 267, 1969–1972.

17 Greczmiel, M.; Strohriegl, P.; Meier, M.; Brutting, W. Macromolecules 1997, 30, 6042–6046.

18 Lee, D. W.; Kwon, K. Y.; Jin, J. I.; Park, Y.; Kim, Y. R.; Hwang, I. W. Chem Mater 2001, 13, 565–574.

19 Shirakawa, H. Angew Chem Int Ed 2001, 40, 2574–2580.

20 Lam, J. W. Y.; Dong, Y.; Kwok, H. S.; Tang, B. Z. Macromolecules 2006, 39, 6997–7003.

21 Yin, S.; Xu, H.; Shi, W.; Gao, Y.; Song, Y.; Lam, J. W. Y.; Tang, B. Z. Polymer 2005, 46, 7670–7677.

22 Yin, S. C.; Xu, H.Y.; Su, X. Y.; Gao, Y.; Song, Y.L.; Lam, J. W. Y.; Tang, B. Z.; Shi, W. Polymer 2005, 46, 10592–10600.

23 Yin, S. C.; Xu, H. Y.; Fang, M.; Shi, W. F.; Gao, Y. C.; Song, Y. L. Macromol Chem Phys 2005, 206, 1549–1557.

24 Yin, S C.; Xu, H. Y.; Su, X. Y.; Li, G.; Song, Y. L.; Lam, J. W. Y.; Tang, B. J Polym Sci Part A: Polym Chem 2006, 44, 2346–2357.

25 Xu, H.Y.; Yin, S.C.; Zhu, W. J.; Song, Y.L.; Tang, B. Z. Polymer 2006, 47, 6986–6992.

26 Tabata, M.; Tanaka, Y.; Sadahiro, Y.; Sone, T.; Yokota, K.; Miura, I. Macromolecules 1997, 30, 5200–5204.

27 Xu, H. Y.; Wang, X.; Wu, J. C. Chin Chem Lett 2008, 19, 141–145.

28 Lam, J. W. Y.; Tang, B. Z. Acc Chem Res 2005, 38, 745–754.

29 Lam, J. W. Y.; Tang, B. Z. J Polym Sci Part A: Polym Chem 2003, 41, 2607–2629.

30 Wang, X.; Wu, J. C.; Xu, H. Y.; Wang, P.; Tang, B. Z. J Polym Sci Part A: Polym Chem 2008, 46, 2072–2083.

31 Wang, X.; Guang, S. Y.; Xu, H. Y.; Su, X. Y.; Yang, J. Y.; Song, Y. L.; Lin, N. B.; Liu, X. Y. J Mater Chem 2008, 18, 4204–4209.

32 Wang, X.; Shen, J.; Wu, J. C.; Fang, M.; Xu, H. Y. Chin Chem Lett 2008, 19, 634–638.

33 Huang, J.; Li, C.; Xia, Y. J.; Zhu, X. H.; Peng, J.; Cao, Y. J Org Chem 2007, 72, 8580–8583.

34 Percec, V.; Rudick, J. G. Macromolecules 2005, 38, 7241–7250.

35 Percec, V.; Rinaldi, P. L. Polym Bull 1983, 9, 548–555.

36 Percec, V.; Rinaldi, P. L. Polym Bull 1983, 9, 582–587.

37 Percec, V. Polym Bull 1983, 10, 1–7.

38 Simionescu, C. I.; Percec, V.; Dumitrescu, S. J Polym Sci: Polym Chem Ed 1977, 15, 2497–2509.

39 Simionescu, C. I.; Percec, V. J Polym Sci: Polym Chem Ed 1980, 18, 147–155.

40 Simionescu, C. I.; Percec, V. J Polym Sci: Polym Lett Ed 1979, 17, 421–429.

41 Rudick, J. G.; Percec, V. Macromol Chem Phys 2008, 209, 1759–1768.

42 Lam, J. W. Y.; Luo, J.; Dong, Y.; Cheuk, K. K. L.; Tang, B. Z. Macromolecules 2002, 35, 8288–8299.

43 Jin, S. H.; Kim, M. Y.; Kim, J. Y.; Lee, K.; Gal, Y. S. J Am Chem Soc 2004, 126, 2474–2480.

44 Meng, H.; Yu, W. L.; Huang, W. Macromolecules 1999, 32, 8841–8847.

45 Percec, V.; Rudick, J. G.; Peterca, M.; Wagner, M.; Obata, M.; Mitchell, C. M.; Cho, W.-D.; Balagurusamy, V. S. K.; Heiney, P. A. J Am Chem Soc 2005, 127, 15257–15264.

46 Yuan, W. Z.; Qin, A.; Lam, J. W. Y.; Sun, J. Z.; Dong, Y.; Haussler, M.; Liu, J.; Xu, H. P.; Zheng, Q.; Tang, B. Z. Macromolecules 2007, 40, 3159–3166.

47 Tan, S.; Zou, Y.; Zhu, W.; Jiang, C. Opt Mater 2006, 28, 1108–1114.

48 Lai, R. Y.; Kong, X.; Jenekhe, S. A.; Bard, A. J. J Am Chem Soc 2003, 125, 12631–12639.

49 Dai, L.; Winkler, B.; Dong, L.; Tong, L.; Mau, A. W. H. Adv Mater 2001, 13, 915–925.

50 Peng, Q.; Lu, Z. Y.; Huang, Y.; Xie, M. G.; Han, S. H.; Peng, J. B.; Cao, Y. Macromolecules 2004, 37, 260–266.

51 Chiu, C. W.; Chow, T. J.; Chuen, C. H.; Lin, H. M.; Tao, Y. T. Chem Mater 2003, 15, 4527–4532.